Journal of Applied Research and Technology

www.jart.icat.unam.mx

Journal of Applied Research and Technology 20 (2022) 48-57

Original

Feasibility of pulsed phase thermography for moisture estimation

A. Fragoso-Mandujano[a] • M. Perez-Patricio[a]* • J. L. Camas-Anzueto[a] •
H. Guerra-Crespo[a] • E. Simá-Moo[b] • Sabino Velázquez-Trujillo[a] • J. B. Hernández-Castillo[c]

[a]*Tecnológico Nacional de México / I T de Tuxtla Gutiérrez, Tuxtla Gutiérrez, Chiapas, Mexico*
[b]*Tecnológico Nacional de México/ CENIDET, Cuernavaca, Morelos, México*
[c]*Tecnológico Nacional de México / I T Tapachula,*
Tapachula de Córdoba y Ordoñez, Chiapas, Mexico

Received 09 21 2020; accepted 05 05 2021
Available 02 28 2022

Abstract: The dehydration of farm products provides farmers an opportunity to preserve their products longer and simultaneously earn more profit from them. Nevertheless, traditionally, the dehydrated products' quality has been determined using invasive methods, for example, through manual measurements with a Vernier caliper and a micrometer. However, manual measurements have their most significant weakness in monitoring continuous production lines and, that is why an efficient methodology is often required for estimating the moisture in dehydrated products. This study aimed to explore the feasibility of pulsed thermography for estimating the moisture content of farm products in the drying process. In this paper, a methodology to estimate dehydration in real-time was developed, and the design and construction of a real-time pulsed thermographic imaging system were described. Moreover, to demonstrate the operation principle, Neem (Azadirachta indica) leaves were used in a dehydration process. The specimen was submitted to a heat pulse, and an infrared camera observed its reaction through time; then, a characteristic curve was generated from the sequence of captured images. That curve relates the moisture content with the response to the heat pulse. The results demonstrated the efficiency of the pulsed thermography in differentiating the percentage of dehydration in Neem leaves

Keywords: Pulsed thermography, Drying, Moisture estimation, Thermal image processing

*Corresponding author.
E-mail address: madain.pp@tuxtla.tecnm.mx (M. Perez-Patricio).
Peer Review under the responsibility of Universidad Nacional Autónoma de México.

1. Introduction

Food drying is one of the most common processes for promoting product stability. The decrease in the amount of water reduces microbial activity and minimizes physical and chemical changes during storage (Mayor & Sereno, 2004). The dehydration process causes changes in food properties, including discoloration, changes in texture and nutritional values, as well as physical changes in appearance and shape. Quality control in the dehydrated products' industry has traditionally been determined using invasive methods (Abasi et al., 2018), for example, through manual measurements with a Vernier caliper and a micrometer, among others. The inspection is based on physical appearance and not on internal properties. In addition, these measurements have been shown to be inadequate because the product is in direct contact with the measuring instrument causing physical damage by the instrument (Jha et al., 2010). Moreover, it has been documented that manual quality control has its greatest weakness in the monitoring of continuous production lines (Mayor & Sereno, 2004). Considering this, nondestructive methods of quality control have been proposed in the literature, some using computer vision systems (CVS) applied to the inspection of fruits (Habib et al., 2018), vegetables (Malekabadi et al., 2017) and leaves (Tech et al., 2018). Nondestructive testing (NDT) provides an alternative to the manual inspection of dehydrated products with the integration of an image acquisition device and a computer (Ferna et al., 2005).

Among the different nondestructive evaluation techniques, pulsed thermography (PT) is a quick evaluation process that uses a high-intensity light source to heat the surface of a specimen (Vavilov & Burleigh, 2015). Short pulses are commonly used, depending on the thermal properties of the object. The evolution of the surface temperature of the sample relative to time is monitored by an infrared (IR) camera with a computer that quantifies the temperature variations of the product (Almond & Pickering, 2012). Changes in the tissue caused by dehydration increase heat conduction, increasing the rate of cooling compared with non-dehydrated tissue. The transient temperature field $\mathbf{T}(z,t)$ in PT is obtained from Eq. 1 which is the solution of the nonhomogeneous one-dimensional (1D) heat conduction equation (Carslaw & Jaeger, 1959):

$$\frac{\partial^2 T(z,t)}{\partial z^2} - \frac{1}{\alpha}\frac{\partial T(z,t)}{\partial t} = -\frac{g(z,t)}{k}, \; t > 0 \tag{1}$$

Where $\alpha = k/\rho c$ is the thermal diffusivity (m^2/s), k is the thermal conductivity (W/mK), ρ is the density (kg/m^3) and c is the specific heat (J/kgK), $g(z,t) = Q_0\delta(z-z)\delta(t-t_0)$ is the external heat impulse located at $z_0 = 0$ and the stimulation time $t_0 = 0$, with Q_0 the intensity of the source per unit length (Jm^{-1}) and $\delta(z-z)\delta(t-t_0)$ Dirac delta in space and time, respectively. Local changes in thermal properties are considered, and they are related to moisture loss and product density change. Changes in moisture levels and product density can be identified by measuring the distribution of surface temperature in the heating and cooling process. Water in intercellular spaces is responsible for increasing density, increasing thermal capacity, decreasing thermal conductivity and thermal diffusivity. Theoretically, by decreasing the moisture content of the product, the density of the product decreases, and consequently, the diffusivity increases. Local changes in thermal properties were considered, and they were related to moisture loss and product density change.

In the agricultural and food industry, PT is particularly suitable in the presence of surface air gaps or internal defects (Wang et al., 2018). For example, the detection of damaged tissues in apples and blueberries (Baranowski et al., 2008, 2009; Kuzy et al., 2018); the identification of foreign matter in cotton (Ginesu et al., 2004; Kuzy & Li, 2017); food quality control (Gowen et al., 2010); the measurement of surface moisture in citrus fruits (Fito et al., 2004); and in the discrimination in the degree of ripeness of tomatoes and apples (Offermann et al., 1998), among others. To the best of the authors' knowledge, however, no studies were found to date that directly relate the estimation of dehydration in agricultural products (fruits, vegetables or leaves) to the PT technique.

On the other hand, the rise of a wide range of development boards in conjunction with open-source software has provided tools to the agricultural sector for the inclusion of new technologies. This has been achieved thanks to the use of simple board computers like Raspberry Pi and also of open-source image processing libraries like OpenCV (Open-Source Computer Vision). In general, previous developments are shifting efforts in precision agriculture towards image-based agricultural product monitoring systems (Osroosh et al., 2018).

This study aimed to explore the feasibility of pulsed thermography for estimating the moisture content of farm products in the drying process. To achieve the objective was developed an algorithm for capturing and analysing thermal images which was implemented in an automatic, fast, and non-destructive imaging system based on pulsed thermography.

2. Materials and methods

2.1. Pulsed thermography imaging acquisition system

For the thermal analysis of the samples, a testing bench of pulsed thermography was built, following the scheme shown in Figure 1, which is an embedded system (Raspberry Pi 3 Model B, Raspberry Pi Foundation) with Python 3 installed as a development language. The images were acquired by a radiometric thermal module without a shutter (FLIR Lepton 2.5, FLIR Systems, Wilsonville, OR, US) mounted on a 10 *cm* long by 10 *cm* high and 10 *cm* deep three-dimensional printed frame (Figure 2).

The FLIR Lepton module has a resolution of 80 x 60 pixels, a spectral range of 8-14 μm and a thermal sensitivity of $0.050\ ^{\circ}C$. A servomotor with a black paper attached is activated when starting the experiment to obtain a reference image in the Lepton module. Four 7W (46823/FI-50T, Voltech, Mexico) crown-like incandescent spotlights mounted on the top lid of the frame provide thermal stimulation. A piece of glass covered with polyethylene foam was chosen as the background for the scene. The polyethylene foam is a thermal insulator, which reduces its heating because of the reflector and maximizes the contrast between the sample and the background. A solid-state relay module (G3MB, Omron, Kyoto, Japan) was used to activate and deactivate the heat source.

In general terms, the system works as follows: The Lepton module is activated, and a black image is acquired as a reference image. The image acquisition is then started, and the servo motor is activated, exposing the module lens while an image of the specimen is captured before stimulation (Figure 3 (a)). The relay is then activated, which turns on the heat source for 11 s. to know the heating time, tests were done at different times and found that the contrast background begins to gain heat in $t > 11\ s$. It is necessary to ensure that the background does not heat up to not introduce errors in the measurements. In this practical way, we determine that 11 seconds is the maximum warm-up time to avoid this phenomenon. Besides, the relay is then deactivated, and the thermal stimulation is completed (Figure 3 (b)). The process finishes 33 s after the heat pulse ends by activating the servomotor, covering the lens, deactivating the Lepton module, and exporting approximately 44 s of video (Figure 3 (c)).

A software application was developed in Python language to automatically operate the system, which consists of the following: activation and deactivation of the reflector, activation and deactivation of the servomotor, thermal camera operation and memory management for storing video.

2.1.1. Sample preparation

This study can be done using several dehydrated agricultural products such as thin layers of fruits, thin layers of vegetables, or leaves. However, Neem (*Azadirachta indica*) leaves were selected because of their availability in the region and their use in traditional medicine to treat skin infections. Another use of Neem is vector control and its potential disease transmission (El et al., 2003). Sixty leaves were collected from the facilities of Tecnológico Nacional de México / I T Tuxtla Gutiérrez in Tuxtla Gutiérrez, Chiapas, in September 2019. The samples were stored for two hours in sealed bags at a constant temperature of $3\ ^{\circ}C \pm 0.10\ ^{\circ}C$ to stabilize their temperature and humidity. The leaves were classified according to a size of approximately 7 $cm \pm$ 0.3 cm in length, and the damaged, withered, or defective leaves were discarded. The selected samples were of similar sizes and had no visible defects, stains, or pests.

For the study, 48 samples were retained. Samples were processed approximately three hours after collection. Two treatment groups were created: the first with 44 samples and the second with four samples as a control group. The first group was dehydrated at $50\ ^{\circ}C$ for 150 min; four samples were taken randomly from every 15 min and evaluated on the testing bench. Finally, the four samples were discarded, and the procedure continues.

2.1.2. Moisture content determination of Neem leaves

To know the moisture of the samples, the leaves were evenly distributed in a tray of a commercial dryer (Hamilton Beach 32100 Food Dehydrator, Hamilton Beach, US) at $50\ ^{\circ}C$ of temperature. A digital scale was used with $\pm$ 0.01 g precision (Mwithiga & Olwal, 2005) to measure the weight of the samples. The samples were dried until the weight readings were constant according to the methodology proposed by (A. O. A. C., 1995). The readings were taken in three replicates, and the average values were used for further analysis.

Usually, the drying curves are expressed by the moisture content (in grams) *X* against time *t*. It is obtained directly from the weight loss and time during drying. Another way to construct the curve is using the moisture ratio (MR) against time t. The MR can be calculated with Eq. 2 (Grumezescu & Holban, 2018):

$$MR = \frac{X - X_{eq}}{X_0 - X_{eq}} \tag{2}$$

where X_0 is the initial moisture content (in grams) and X_{eq} is the moisture content in balance (in grams). If X_{eq} is very small compared with X_0, Eq. 2is simplified as Eq.3.

$$MR \approx \frac{X}{X_0} \tag{3}$$

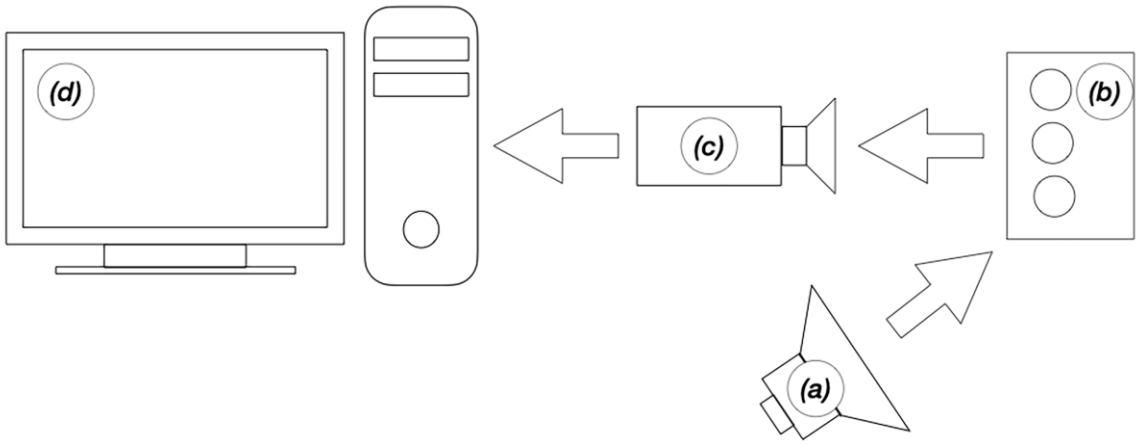

Figure 1. General configuration of experiments in active thermography:
(a) heat source, (b) specimen, (c) infrared camera, and
(d) embedded system for displaying, recording and processing data.

2.2. Processing of thermal images

The processing of the information was carried out in four stages: a) image capture (Figure 4(a)), b) extraction of the region of interest (Figure 4(b)), c) plotting of the thermal kinetics curve and curve feature extraction (Figure 4(c)), and d) classification (Figure 4(d)). Each of these steps are detailed below.

2.2.1. Imaging capture

The duration of the obtained videos was 44 s. One second after calibrating the module with the black image and starting the recording, the servomotor is activated by uncovering the lens and activating the heat source. At 12 s, the heat source is deactivated, resulting in a total heat pulse duration of 11 s. After 43 s of starting the recording, the servomotor is activated again to cover the lens, giving 31 s of a cooling curve. The recording is finished with an additional second of image capture to avoid unintentional truncation of information. The eight first samples information captured was intertwined: First, a video was captured from the control sample (fresh leaves), followed by the sample from the dry leaves group. The rest of the information capture was taken from the samples of the group of dry leaves. One video was obtained per sample, producing 48 videos in total where each video was captured at 20 FPS, yielding approximately 42,000 images to process.

2.2.2. Extraction of the region of interest

The extraction of the region of interest aims to highlight the relevant areas in the scene. The image segmentation favors the algorithm's simplicity, the speed of execution, the computing charge, and the correct segmentation to avoid modifying the FLIR module's original information. Finally, the results obtained with the aid of segmentation minimize the noise presented in the region of interest instead of not segmenting the image.

The segmentation process was performed using the scikit image library for Python. A three-dimensional matrix $T(x,y,z) \in R^{mxnxp}$ was obtained from the sequence of captured images. All the pixels of each image were averaged (Eq.4), and the maximum temperature value index (Eq.5) was sought:

$$\bar{a}_k = \frac{1}{n \cdot m} \sum_{i=1}^{m} \sum_{j=1}^{n} T_{i,j},\ For\ k = 1,2,3,4,\dots,p \tag{4}$$

$$t_{max} = index\left(max\left\{\overline{a_1}, \overline{a_2}, \overline{a_3}, \dots, \overline{a_p}\right\}\right) \tag{5}$$

The image that matches the peak temperature $P(x,y,t_{max})$ was segmented by thresholding, given the transformation function (Eq.6) where the transition level given by the parameter $threshold = 10$ In the inspection of 48 samples, we found that, on average, the contour of the leaves had a mean value of 10 on a grayscale, which allowed us to delimit the edges for the binarization and information extraction process. This value must be calibrated for each different product.

$$q(x,y) = \begin{cases} 0 & to\ \ p(x,y,t_{max}) \leq threshold \\ 255 & to\ \ p(x,y,t_{max}) > threshold \end{cases} \tag{6}$$

The number of white pixels (WP) was counted to know the total of pixels in the region of interest with Eq. 7.

$$WP = \sum_{i=1}^{m} \sum_{j=1}^{n} q_{i,j} \tag{7}$$

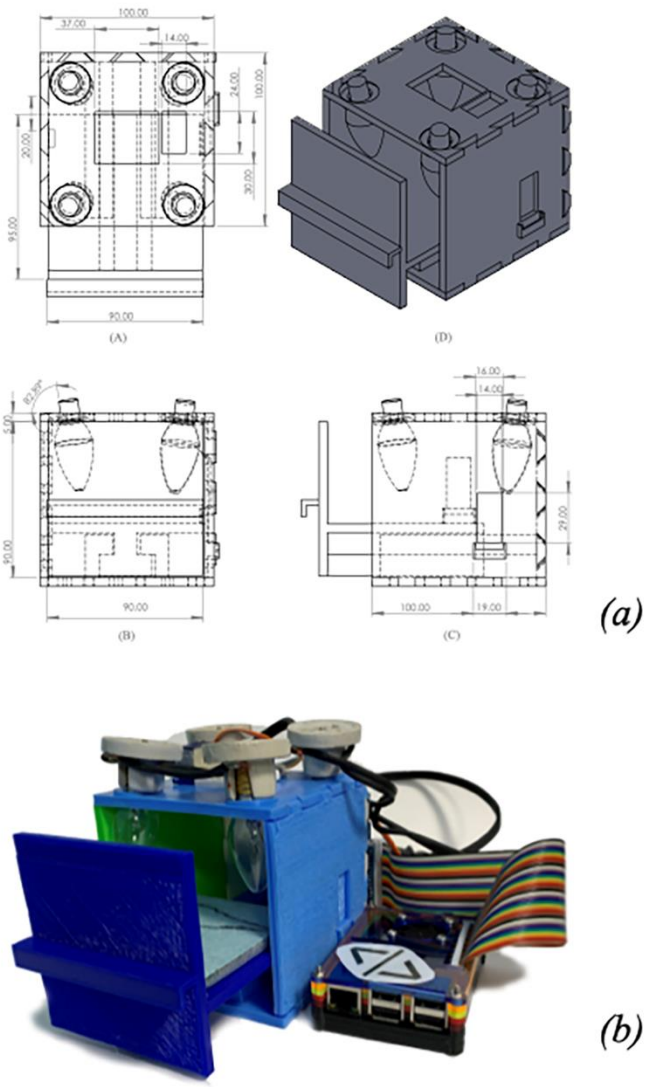

Figure 2. Testing bench design overview: (a) testing bench side views and isometric views and (b) part assembly.

The segmented image ($q(x,y)$) was multiplied by each frame in the video to extract only the pixels of the leaves according to Eq.8. All the pixels of the object are averaged together with Eq.9, which produces an average value for each frame. In addition, the temperature variation (Eq.10) was plotted with respect to time. The set of values that were obtained from Eq. 10were stored in CSV formatted files for analysis.

$$Q(x,y,z) = T(x,y,t) \cdot q(x,y) \tag{8}$$

$$\bar{b}_k = \frac{1}{WP}\sum_{i=1}^{m}\sum_{j=1}^{n} Q_{i,j}, For\ k = 1,2,3,4,\ldots,p \tag{9}$$

$$\bar{B} = \{\bar{b}_1, \bar{b}_2, \bar{b}_3, \ldots, \bar{b}_p\} \tag{10}$$

2.2.3. Thermal curve profile, amplitude, and phase extraction

Pulsed phase thermography (PPT) is an analytical technique for analyzing the thermal response from the object to the heat pulse. In this technique, the grayscale intensity change of each pixel of the object was considered as a temporary thermal signal. The series of input signals is known as the thermal profile curve. The Fourier discrete-time transformation (DFT) decomposes the input signal given by the thermal profile curve into a sum of sinusoidal components, each having a different frequency, amplitude, and phase delay. The infinite integral of exponential functions expresses the continuous Fourier transform (Baranowski et al., 2009) as shows in Eq. 11:

$$F(v) = \int_{-\infty}^{\infty} f(t) e^{(-j2\pi vt)}\, dt \tag{11}$$

where $j^2 = -1$. When a finite series of signal samples $(T_0, T_1, T_2, \ldots, T_{N-1})$ is analyzed, it can be transformed into a fundamental frequency (F_0) and harmonic series $(F_1, F_2, F_3, \ldots, F_{N-1})$ (Brown & Puckette, 1993) by using the Eq. 12:

$$F_n = \sum_{k=0}^{N-1} T_k e^{(-j2\pi nk/N)} = \mathrm{Re}_n + \mathrm{Im}_n \tag{12}$$

where Re and Im are the real and imaginary components of the transform, respectively, j is an imaginary unit, n is the number of harmonic components $(n = 0,1,\ldots,N)$, k is the signal sample's value. The real and imaginary part of the DFT can be used to calculate the amplitude with Eq. 13and with Eq. 14 the phase delay of the thermal profile curve. The phase delay that corresponds to the fundamental frequency is of interest among researchers as characteristics of the samples' discrimination (Brown & Puckette, 1993; Kamarainen et al., 2002; Kuzy & Li, 2017).

$$A_n = \sqrt{Re_n^2 + Im_n^2} \tag{13}$$

$$\phi_n = tan^{-1}\left(\frac{Im_n}{Re_n}\right) \tag{14}$$

Fourier's analysis of the samples was done using the Python NumPy library. The Fourier's analysis input signal was thermal profile waves shown in Figure 6. Followed by the Fourier decomposition, several complex components equal to the number of frames in each video were generated. The Hermite function's symmetry properties are reflected in the amplitude and phase transformation, which are even and odd, respectively, concerning $f = 0$ Hz.

Therefore, for a sequence of N thermograms, there are $N/2$ proper frequencies ($10\ Hz$); the other half of the spectrum provides redundant information that can be dismissed. The fundamental frequency phase is interesting since it is less

affected by the typical problems of active thermography such as the noise present in the measurements, reflections from the environment, variations in emissivity, and non-uniform heating, among others (Ibarra-Castanedo et al., 2014).

2.2.4. Feature selection and estimation of MR

In previous studies, (Kuzy & Li, 2017) determined that the set of characteristics in the frequency domain is suitable for discriminating between materials. For this study, the phase of the fundamental frequency obtained from Eq. 14 was selected to estimate leaf moisture during the dehydration process. Moreover, when the amplitude and phase information was analyzed, it was found that the amplitude does not provide enough information to discriminate degrees of dehydration; that is why it was considered to take only the phase information. The estimation was made using a curve adjusted to the values given by the phase of the fundamental frequency and the moisture percentage given in Figure 5.

3. Results and discussion

3.1. Drying of leaves

The weight difference of the leaves as a function of time throughout the drying process was monitored. Figure 5 shows the drying curve for Neem leaves at $50\ °C$. The initial drying speed was high because of the product's high moisture content and the high temperature inside the dryer. The drying speed decreased continuously in proportion to the decrease in the humidity of the leaves. Drying time for the constant temperature of $50\ °C$ was 165 min When compared to previous studies on fruits, vegetables and leaves, this curve is in good agreement (Ali et al., 2014).

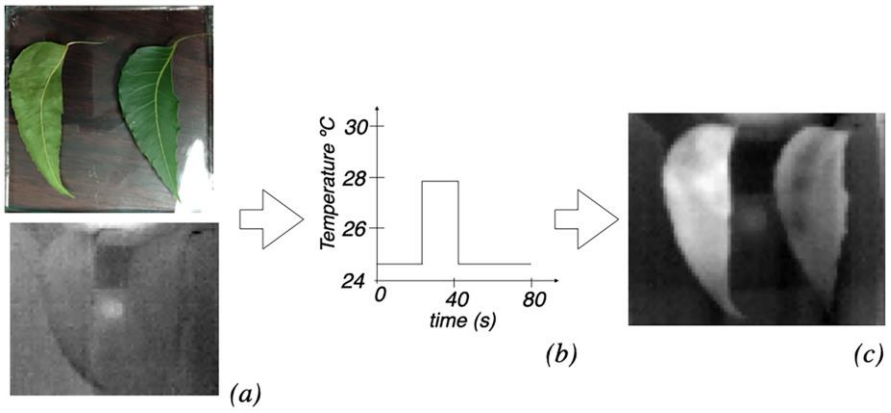

Figure 3. General scheme of active thermography where as can be seen (a) thermal images of the specimen prior to the heat pulse, (b) the heat pulse and (c) the surface response of the product to thermal stimulation.

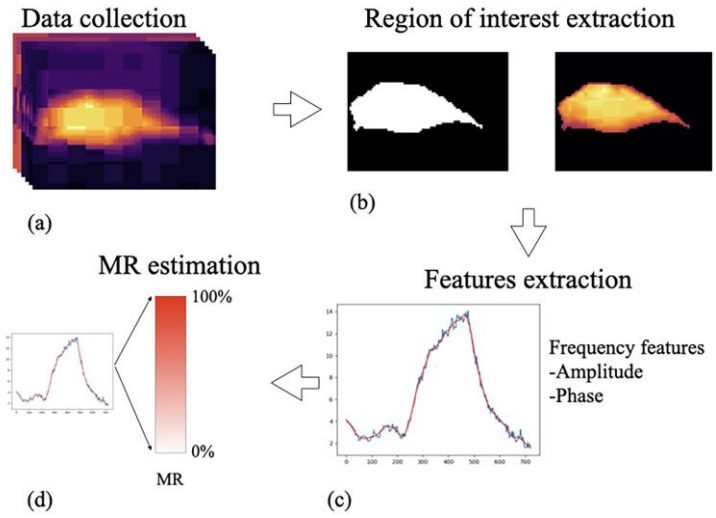

Figure 4. General overview of information processing.

Figure 5 shows the moisture content of the product concerning the drying time, at constant temperature and constant airflow. The curve fit was made with a second-order polynomial regression, giving the equation $\%MR = 0.0033t^2 - 1.1114t + 96$ with R^2 of 0.97.

3.2. Analysis of the thermal profile curve

Concerning the curves of Figure 6 during the stage where the drying speed decreases, most of the curves of thermal kinetics are found. There is a difference from one another, and in the phase of high drying speed a wider difference is shown between curves of thermal kinetics.

As can be seen, Figure 6 shows the response of the Neem leaves to thermal stimulation. Each dehydration degree's thermal profile wave shown in Figure 6 presents a difference between the curves at different dehydration levels of the product. For example, the peak gray value of the sample MR 6%, with a mean value of 14.8 ≈ 15 in grayscale, was higher than MR 48% that had a maximum average value of 10.07 ≈ 10 in grayscale. It can be observed that the samples between MR 48 % and MR 21% reach similar maximum levels; however, the heating and cooling zone have different gradients.

From the set of curves of Figure 6, it is observed that at the beginning of the thermal kinetic curves from $t_0 = 0\ s$ to $t_1 \approx 1.4\ s$, there is an abrupt rise in intensity. This directly corresponds to the reference image's capture and to the activation of the servomotor to discover the lens of the FLIR module.

Similarly, between the time $t_2 \approx 42\ s$ and $t_3 = 44.05\ s$, a rapid drop is observed in the average gray value within the region of interest, and this drop corresponds to the shutter closure of the FLIR module.

3.3. Leaves moisture estimation

The fundamental frequency phase shifts between the thermal kinetic curves are evidenced by the time variation between the maximum gray values within the region of interest. The samples that reach high temperatures the fastest are the most dehydrated. The phase change is represented by a variation in the time axis of the thermal kinetic curve.

As was previously mentioned, the phase of the fundamental frequency was selected as an estimation parameter, and the drying curve (Figure 5) was related to each percentage of dehydration corresponding to a value of the phase of the fundamental frequency of each test. This relation was plotted, and nonlinear regressions were calculated to find the one that best fits the data. The equation that best fits the data is the one proposed in this study, Eq.15, had a R-square of 0.8937 and RMSE of 8.8313, where $\%MR$ is the estimated moisture percentage and ϕ_n is the phase calculated by Eq. 14.The data and the fit curve are shown in Figure 7.

$$\%MR = 149.81e^{-1.625\phi_n - 0.119} \quad (15)$$

To validate the estimation equation, 36 Neem leaves were dried at $50\ ^\circ C$, and groups of three leaves were removed every 15 min and submitted to the estimation system. The precision in the estimation given by Eq. 15 was 85.3%.

With the algorithm implemented in the proposed device, the average processing time of the sequence of images (approximately 880 images) was 0.8812 s. On the other hand, the average time of capturing images was 44 s, giving an overall average of the estimation process of approximately 45 s. Furthermore, because of the time of capture and image processing is very short compared to the time during the drying process, the method presented in this work could be used in a processing line for dehydrated products.

The methodology developed in this work could be applied to other agricultural products. Thermal curves will be obtained that relates the variation of the moisture of the product during the drying process and the response in phase according to each product.

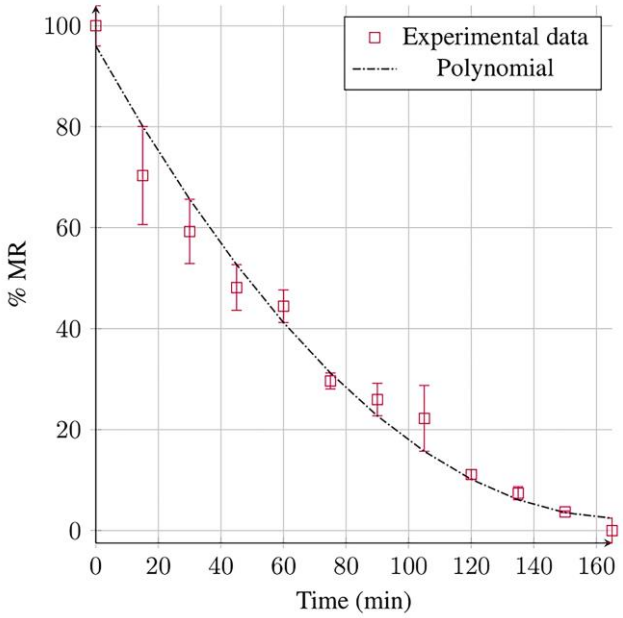

Figure 5. Neem's drying curve at 50°C.

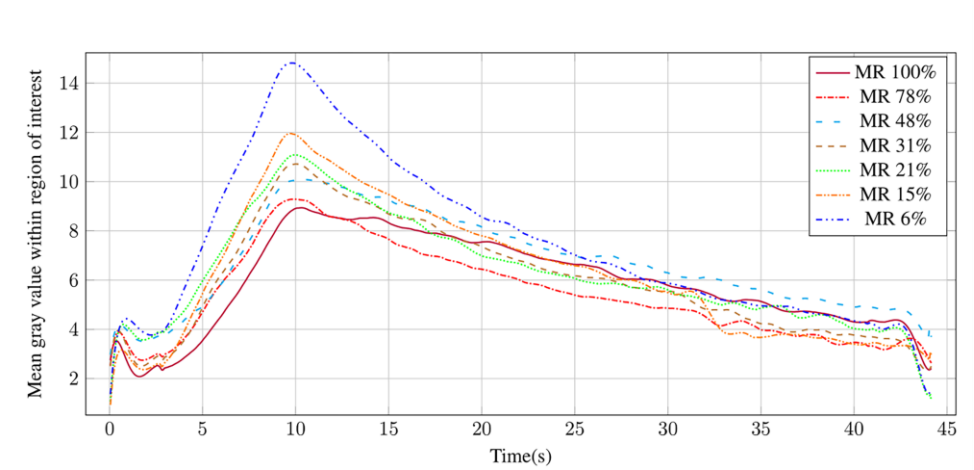

Figure 6. Thermal profile waves of all study samples.

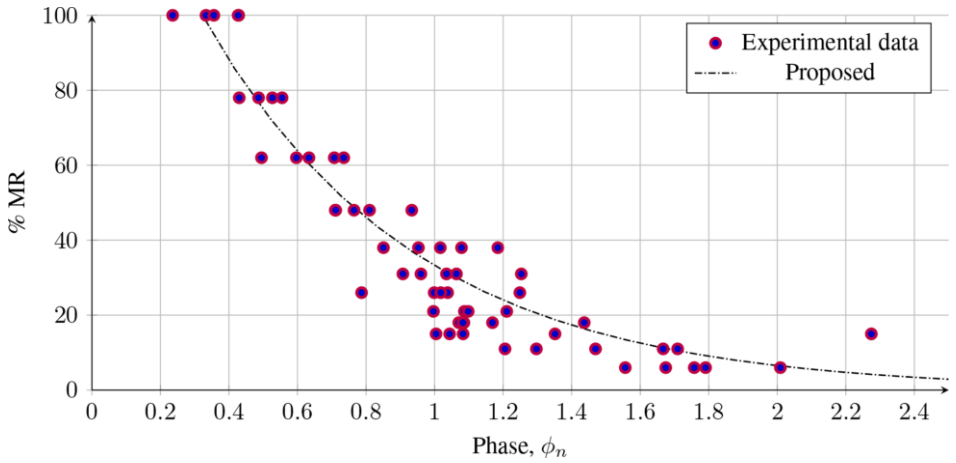

Figure 7. Drying estimation curve.

4. Conclusions

The obtained results demonstrate that pulsed thermography is a viable method for estimating dehydration in Neem leaves. In addition, the imaging system based on pulsed thermography developed in this work proved to be effective in estimating levels of dehydration in Neem leaves. The estimation equation that was proposed for the dehydration estimation produces results with more than 80% precision using the set of characteristics related to the fundamental frequency phase as well. Because of the simplicity of the algorithm, it can run on a Raspberry Pi 3 Model B, with a low-computing charge for the development board. Finally, the proposed methodology can be applied to various dehydrated agricultural products such as fruits and vegetables.

Conflict of interest

The authors does not have any type of conflict of interest to declare.

Acknowledgments

Fragoso-Mandujano thanks the Consejo Nacional de Ciencia y Tecnologia (CONACyT, Mexico), and TecNM / ITTG computer vision team facilities.

Financing

The authors did not receive any sponsorship to carry out the research reported in the present manuscript.

References

Abasi, S., Minaei, S., Jamshidi, B., & Fathi, D. (2018). Dedicated non-destructive devices for food quality measurement: A review. *Trends in Food Science and Technology*, *78*, 197–205 https://doi.org/10.1016/j.tifs.2018.05.009

Ali, M. A., Yusof, Y. A., Chin, N. L., Ibrahim, M. N., & Basra, S. M. A. (2014). Drying Kinetics and Colour Analysis of Moringa Oleifera Leaves. *Agriculture and Agricultural Science Procedia*, *2*, 394–400. https://doi.org/10.1016/j.aaspro.2014.11.055

Almond, D. P., & Pickering, S. G. (2012). An analytical study of the pulsed thermography defect detection limit. *Journal of Applied Physics*, *111*(9). https://doi.org/10.1063/1.4704684

Baranowski, P., Lipecki, J., Mazurek, W., & Walczak, R. T. (2008). Detection of watercore in "Gloster" apples using thermography. *Postharvest Biology and Technology*, *47*(3), 358–366. https://doi.org/10.1016/j.postharvbio.2007.07.014

Baranowski, P., Mazurek, W., Witkowska-Walczak, B., & Sławiński, C. (2009). Detection of early apple bruises using pulsed-phase thermography. *Postharvest Biology and Technology*, *53*(3), 91–100. https://doi.org/10.1016/j.postharvbio.2009.04.006

Brown, J. C., & Puckette, M. S. (1993). A high-resolution fundamental frequency determination based on phase changes of the Fourier transform. *Journal of the Acoustical Society of America*, *94*(2), 662–667. https://doi.org/10.1121/1.406883

Carslaw, H.S.; Jaeger, J. C. (1959). *Conduction ofHeat in Solids* (Clarendon Press, Ed.; 2nd ed).

El, A., El, M., Hamed, I., Rhee, K., Ahmed, A., Zeller, P., & Verpoorte, R. (2003). Bioactive constituents of neem. In *Fitoterapia* (Vol. 74). Elsevier Ltd.

Ferna, L., Castillero, C., & Aguilera, J. M. (2005). An application of image analysis to dehydration of apple discs. *Journal of Food Engineering 67*, *67*, 185–193. https://doi.org/10.1016/j.jfoodeng.2004.05.070

Fito, P. J., Ortolá, M. D., de los Reyes, R., Fito, P., & de los Reyes, E. (2004). Control of citrus surface drying by image analysis of infrared thermography. *Journal of Food Engineering*, *61*(3), 287–290. https://doi.org/10.1016/S0260-8774(03)00120-1

Ginesu, G., Giusto, D. D., & Meinlschmidt, P. (2004). Detection of Foreign Bodies in Food by Thermal Image Processing. *IEEE Transactions on Industrial Electronics*, *51*(2), 480–490. https://doi.org/10.1109/TIE.2004.825286

Gowen, A. A., Tiwari, B. K., Cullen, P. J., McDonnell, K., & O'Donnell, C. P. (2010). Applications of thermal imaging in food quality and safety assessment. Trends in food science & technology, 21(4), 190-200. https://doi.org/10.1016/j.tifs.2009.12.002

Grumezescu, A. M., & Holban, A. M. (2018). Natural and Artificial Flavoring Agents and Food Dyes. In Natural and Artificial Flavoring Agents and Food Dyes, 21-24.

Habib, M. T., Majumder, A., Jakaria, A. Z. M., Akter, M., Uddin, M. S., & Ahmed, F. (2018). Machine vision-based papaya disease recognition. *Journal of King Saud University - Computer and Information Sciences, 32*(3), 300-309. https://doi.org/10.1016/j.jksuci.2018.06.006

Ibarra-Castanedo, C., González, D. A., Hakim Bendada, & Xavier Maldague. (2014). Análisis de imágenes en Termografía Infrarroja. Laboratoire de Vision et Systèmes Numériques de l'Université Laval, 5.

Jha, S. N., Narsaiah, K., Sharma, A. D., Singh, M., Bansal, S., & Kumar, R. (2010). Quality parameters of mango and potential of non-destructive techniques for their measurement—a review. *Journal of food science and technology, 47*(1), 1-14. https://doi.org/10.1007/s13197-010-0004-6

Kamarainen, J., Kyrki, V., & Kalviainen, H. (2002, August). Fundamental frequency Gabor filters for object recognition. In *Object recognition supported by user interaction for service robots 1*, 628-631. IEEE. https://doi.org/10.1109/ICPR.2002.1044822

Kuzy, J., Jiang, Y., & Li, C. (2018). Blueberry bruise detection by pulsed thermographic imaging. *Postharvest Biology and Technology, 136*, 166-177. https://doi.org/10.1016/j.postharvbio.2017.10.011

Kuzy, J., & Li, C. (2017). A pulsed thermographic imaging system for detection and identification of cotton foreign matter. *Sensors, 17*(3), 1–15. https://doi.org/10.3390/s17030518

Malekabadi, A. J., Khojastehpour, M., Emadi, B., & Golzarian, M. R. (2017). Development of a machine vision system for determination of mechanical properties of onions. *Computers and Electronics in Agriculture, 141*, 131-139. https://doi.org/10.1016/j.compag.2017.07.016

Mayor, L., & Sereno, A. M. (2004). Modelling shrinkage during convective drying of food materials: A review. *Journal of Food Engineering, 61*(3), 373–386. https://doi.org/10.1016/S0260-8774(03)00144-4

Mwithiga, G., & Olwal, J. O. (2005). The drying kinetics of kale (*Brassica oleracea*) in a convective hot air dryer. *Journal of Food Engineering, 71*(4), 373–378. https://doi.org/10.1016/j.jfoodeng.2004.10.041

O. A. C. (1995). *Official Temperatures of Analysis of the Association of Official Analytical Chemists* (16th editi, Vol. 1, Issue Volume 1).

Offermann, S., Bicanic, D., Krapez, J. C., Balageas, D., Gerkema, E., Chirtoc, M., Egee, M., Keijzer, K., & Jalink, H. (1997). Infrared transient thermography for non-contact, nondestructive inspection of whole and dissected apples and of cherry tomatoes at different maturity stages. *Instrumentation Science and Technology, 26*(2–3), 145–155. https://doi.org/10.1080/10739149808002689

Osroosh, Y., Khot, L. R., & Peters, R. T. (2018). Economical thermal-RGB imaging system for monitoring agricultural crops. *Computers and Electronics in Agriculture, 147*,34–43. https://doi.org/10.1016/j.compag.2018.02.018

Tech, A. R. B., Silva, A. L. C. da, Meira, L. A., Oliveira, M. E. de, & Pereira, L. E. T. (2018). Methods of image acquisition and software development for leaf area measurements in pastures. Computers and Electronics in Agriculture, 153, 278–284. https://doi.org/10.1016/j.compag.2018.08.025

Vavilov, V. P., & Burleigh, D. D. (2015). Review of pulsed thermal NDT: Physical principles, theory and data processing. *NDT and E International, 73*, 28–52. https://doi.org/10.1016/j.ndteint.2015.03.003

Wang, Z., Tian, G., Meo, M., & Ciampa, F. (2018). Image processing based quantitative damage evaluation in composites with long pulse thermography. *NDT & E International, 99*, 93–104. https://doi.org/10.1016/j.ndteint.2018.07.004